Stationary, dynamical, and chaotic states of the two-dimensional damped Kuramoto-Sivashinsky equation

Marco Paniconi[1] and K. R. Elder[2]
[1]*Department of Physics and Beckman Institute, 1110 West Green Street, University of Illinois at Urbana-Champaign, Urbana, Illinois 61801-3080*
[2]*Department of Physics, Oakland University, Rochester, Michigan 48309-4401*
(Received 28 February 1997)

The long-time behavior of the two-dimensional damped Kuramoto-Sivashinsky equation is studied numerically in the large-aspect-ratio limit. The equation is shown to lead to three states depending on the magnitude of a damping parameter α. At large, intermediate, and small values of α, the equation leads respectively to hexagonal, breathing hexagonal, and disordered states. The disordered phase is chaotic in both space and time, consistent with spatiotemporal chaos. The transitions between these states are examined using standard statistical measures. [S1063-651X(97)06709-3]

PACS number(s): 05.45.+b

I. INTRODUCTION

The appearance of spatially and temporally coherent cellular states is a common feature of many driven nonequilibrium systems, such as directional solidification [1–5], Rayleigh-Bénard convection [6–8], parametrically excited surface waves or Faraday waves [9–11], and electroconvection in liquid crystals [12]. These cellular states arise from a symmetry breaking of a homogeneous spatially extended system through primary instabilities, such as the Mullins-Serkerka [1] instability in directional solidification and the Faraday instability [13] in parametrically excited surface waves. Perhaps more interestingly, there exist secondary instabilities that can destroy the ordered cellular states and give rise to phases that are disordered in both space and time. In directional solidification [3–5] the secondary instabilities include breathing and solitary modes, tip splitting, and birth and death sequences, while in Faraday waves [9] the secondary instabilities include Eckhaus, zigzag, and transverse amplitude modulations. There are a vast number of such phenomena occurring in widely varying fields. An extensive review of such far from equilibrium phenomena is given by Cross and Hohenberg [14].

The generic feature of these systems is that under certain conditions (typically large driving forces) the periodic or regular structures become dynamically unstable and appear to be disordered or ''chaotic'' in both space and time. In spatially extended systems, or in the large-aspect-ratio limit (i.e., when the system size is much greater than the periodicity of the cellular patterns), this behavior is commonly referred to as spatiotemporal chaos or weak turbulence [15,16,22]. The nonstationary chaotic states are somewhat reminiscent of single-phase equilibrium states in that correlations decay exponentially in both space and time. In this paper a simple equation that describes such behavior, namely, the damped or stabilized Kuramoto-Sivashinsky (DKS) [17,18] equation, is examined. While it is unlikely that all the nonequilibrium systems discussed above can be described by a single ''generic'' model, the DKS equation displays many of the secondary instabilities seen in directional solidification and provides a simple mathematical model for studying the selection of nonequilibrium states and the transition to spatiotemporal chaos from a coherent cellular state. It has also been argued [19,20] that this equation (and slightly modified versions) serves as a generic model of systems with broken parity symmetry and should be relevant for directional solidification fronts.

The main focus of this paper is a statistical characterization of the states selected by the two-dimensional DKS equation from a random initial condition in the large-aspect-ratio limit (i.e., when the system size is far greater than the size of the cellular structures). This study compliments an earlier study [21] of the one-dimensional DKS equation. The main result of this earlier study was the observation of a discontinuous transition from stationary periodic states to spatiotemporal chaos. It is improbable that this result will apply in higher dimensions. Even in equilibrium systems, it is well known that spatial dimension plays a strong role in state selection and in the nature of transitions between phases. Our main finding in this paper is the existence of a different nontrivial asymptotic state, at intermediate values of the damping parameter α, that is hexagonally ordered and vacillates or breathes in time. For larger and smaller values of α, hexagonal and spatiotemporal chaotic states are respectively observed. A characterization of the various states based on static and dynamic structure factors is used to establish the phase diagram of this system. To our knowledge, this is the first study of the DKS equation in two dimensions.

The difficulty in predicting the selected asymptotic states and the nature of the transition between these states is that the dynamics are inherently nongradient, i.e., there does not exist a free energy or Lyapunov functional. In addition, spatiotemporal chaos appears in the absence of thermal fluctuations (at least in the theoretical models). Under these conditions there is no criterion for determining the selected states. Nevertheless, it is interesting to note that even within equilibrium theory the transition from one dimension to two dimensions leads to significantly different behavior since only disordered states can exist in one dimension at finite temperature. Thus it is expected that the DKS equation will display much richer behavior in two dimensions than in one.

In the next section the one-dimensional DKS equation is introduced and extended to two dimensions. A brief description of related work is also given. In Sec. III the numerical simulations of the two-dimensional DKS equation are presented. Finally, in Sec. IV a discussion and summary of these results are given.

II. MODEL

The one-dimensional damped Kuramoto-Sivashinsky equation can be written as

$$\partial_t h(x,t) = -(\alpha + \partial_x^2 + \partial_x^4) h(x,t) + [\partial_x h(x,t)]^2, \qquad (1)$$

where $\partial_x \equiv \partial/\partial x$ and $\partial_t \equiv \partial/\partial t$. To the limited extent that this model describes directional solidification, the field $h(x,t)$ represents the position of the liquid-solid interface and the damping factor α is related to the driving force. Increasing the distance from the primary instability (i.e., increasing $\alpha_c - \alpha$, where $\alpha_c = 1/4$ is where the primary instability occurs) eventually drives the system chaotic. This equation can be easily extended to higher dimensions by replacing one-dimensional derivatives (i.e., ∂_x) with gradients (i.e., $\vec{\nabla} \equiv \hat{x}\partial_x + \hat{y}\partial_y + \cdots$),

$$\partial_t h(\vec{r},t) = -(\alpha + \nabla^2 + \nabla^4) h(\vec{r},t) + |\vec{\nabla} h(\vec{r},t)|^2, \qquad (2)$$

where $\nabla^2 \equiv \partial_x^2 + \partial_y^2 + \cdots$. In this paper the late time solutions of Eq. (2) are examined in two dimensions for a spatially extended system.

Equation (2) contains a primary (linear) instability to the formation of periodic structures of wave vector $k_L = 1/\sqrt{2}$ for $\alpha < \alpha_c = 1/4$. For α just below α_c, this instability leads to stationary periodic patterns. In one dimension the dynamic stability of these patterns has been studied extensively by Misbah and Valance [17]. In that work they found a band of stable periodic states just below the primary instability centered around k_L. As the damping parameter α is decreased, several interesting secondary instabilities, in addition to the usual Eckhaus instability, were found to arise, such as parity-breaking modes, vacillating breathing modes, and period halving. While that study examined the stability of the stationary solutions, the selection of states was not considered.

The first examination of the selection of states was undertaken numerically by Chaté and Manneville [18]. In that work they found that just below the primary instability the asymptotic solutions (starting from a random initial condition) led to periodic stationary solutions. Far below the primary instability they found chaotic solutions. It was originally conjectured [18] that the transition from periodic to chaotic states was continuous (second order), based on the continuous decrease of the lamellar-chaotic front velocity as the transition is approached and on the nonexponential decay of lamellar domain sizes at the transition. More recent discussions of the DKS equation by Manneville [22] admit the possibility of a first-order transition. Recently, a numerical finite-size scaling analysis [21] on a discrete map lattice version of the DKS equation provided strong evidence of a first-order or discontinuous transition. The transition to spatiotemporal chaos was found to be coincident with the appearance of the so-called breathing modes (which corresponds to a periodic oscillation of the patterns). In the next section the two-dimensional behavior of the DKS equation is examined.

III. NUMERICAL SIMULATIONS

The two-dimensional DKS equation (2) was numerically integrated using Euler's method for the time derivative on a spatial mesh of size $dx = 1.0$ and time step $dt = 0.035$. The first-order spatial derivatives were evaluated by the usual midpoint discretization, and an isotropic form [23] was used for the Laplacian. This discretization is by no means meant to actually solve the continuum equations, but rather to qualitatively capture the essential features of the underlying continuum model. The numerical method was chosen explicitly to study the late-time large-aspect-ratio limit. Test simulations were conducted for a smaller mesh size ($dx = 0.5$ and $dt = 0.005$). No significant change in the system behavior was observed. For the one-dimensional DKS [21], a similar discretization of the equation yielded the same basic steady states and instabilities of the continuum model numerically studied by Misbah and Valance [17]. No new phenomenon, beyond what was seen in the solutions of the continuum model, was observed with the discrete model. In two dimensions the present discretization should capture the salient features of the two-dimensional DKS equation.

A periodic system of size $L = 512$ was studied. Each run started from a random initial state with a small noise amplitude of approximately 0.01. The aspect ratio for $L = 512$ is about 57 (the typical pattern size has wave number $k \approx 1/\sqrt{2}$).

A. Qualitative characterization

The numerical simulation of Eq. (2) led to three distinct solutions in the late time limit, depending on the magnitude of the control parameter α. At ''large'' values of α (i.e., $0.2176 < \alpha < 0.25$) a periodic hexagonal morphology emerges. An example of such a morphology is shown in Fig. 1(a) for $\alpha = 0.225$ at $t = 35\,000$. Defects are clearly evident in the pattern, such as point defects (the destruction of a hexagon) and line defects that separate domains that are characterized by a fixed hexagon orientation. As α is decreased, the hexagonal state begins to oscillate or breathe in time. In this state each cell oscillates out of phase with its nearest neighbors, so that at a given instant there is a pattern of larger and smaller cell sizes. An example of such a state is shown in Fig. 1(b) for $\alpha = 0.210$ at $t = 35\,000$. As the damping parameter α is reduced further, the breathing or oscillation of the cells eventually becomes large enough to generate a spatiotemporal chaotic state. In this regime the system is disordered in both space and time. A typical example is displayed in Fig. 1(c) for $\alpha = 0.195$ at $t = 35\,000$. A larger variation of cell size and shape can be seen. For purposes of identification the large-, intermediate-, and small-α states will be respectively referred to as ''hexagonal,'' ''breathing hexagonal,'' and ''chaotic'' states. The transition from spatiotemporal chaos to the breathing hexagonal state occurs at $\alpha_{CB} \approx 0.207$ and the transition from breathing hexagonal to hexagonal states occurs at $\alpha_{BO} \approx 0.2176$.

The qualitative difference between the three states is further illustrated in Fig. 2, in which the dynamics of a single

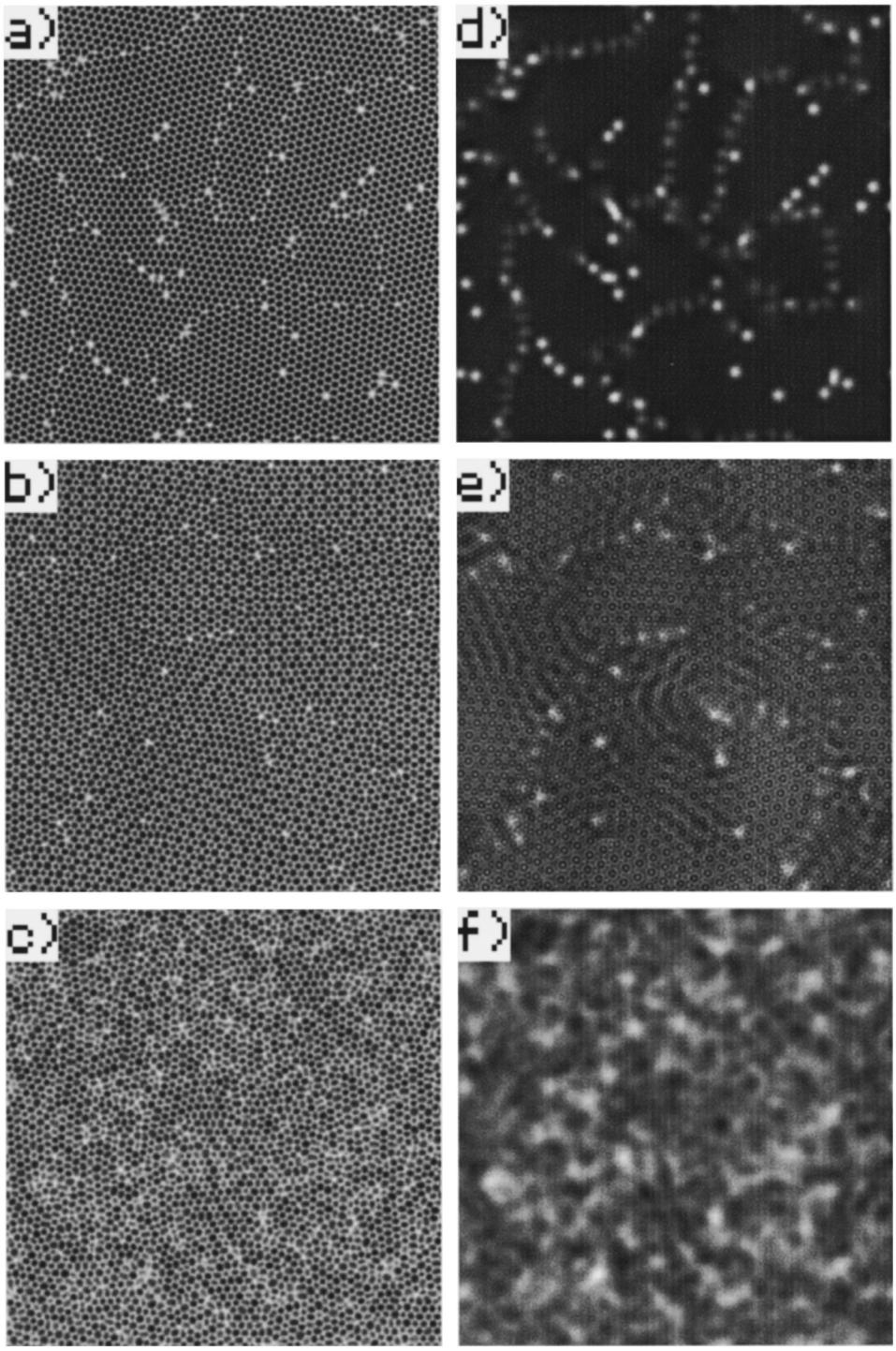

FIG. 1. Spatial configurations at $t=35\,000$ (1×10^6 iterations): (a) hexagonal state, $\alpha=0.225$; (b) breathing hexagonal state, $\alpha=0.210$; and (c) spatiotemporal chaotic state, $\alpha=0.195$. (d), (e), and (f) Fourier filtered configurations for the same states as in (a), (b), and (c), respectively.

Fourier mode $\hat{\psi}(k_x,k_y,t)$ of the order parameter is displayed, where $\hat{\psi}(k_x,k_y,t)$ is the discrete spatial Fourier transform of $\psi(idx,jdx,t)$,

$$\hat{\psi}(k_x,k_y,t)=\sum_{i,j} e^{\sqrt{-1}(ik_x+jk_y)dx}\psi(idx,jdx,t). \qquad (3)$$

The summations i and j run over the entire lattice of size L, giving a finite-size resolution in k space of $2\pi/512$. In Fig. 2 a typical Fourier mode is shown for the three different states as a function of time [note the different scale for Fig. 2(a)]. For the $\alpha>\alpha_{BO}$, $\hat{\psi}(k_x,k_y,t)$ varies slowly in time. This slow variation is due to the slow motion of defects. For the breathing state (i.e., $\alpha=0.210$), a clear periodic oscillation is observed corresponding to the breathing of the cells. Finally, for small α (i.e., $\alpha=0.195$) the dynamics becomes chaotic, as can be seen in Fig. 2(c).

To more accurately characterize the states the circularly

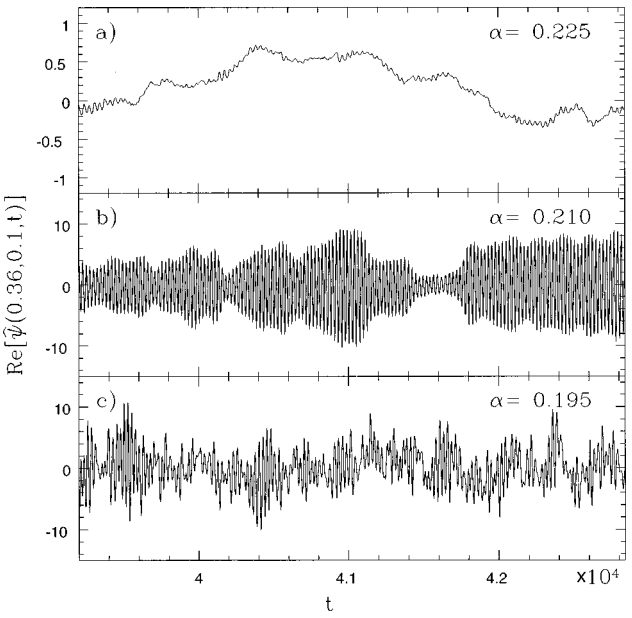

FIG. 2. Time series for a Fourier mode $\mathrm{Re}\psi(\vec{k})$, for $\vec{k}=(0.36,0.1)$, as a function of time: (a) $\alpha=0.225$, (b) $\alpha=0.210$, and (c) $\alpha=0.195$.

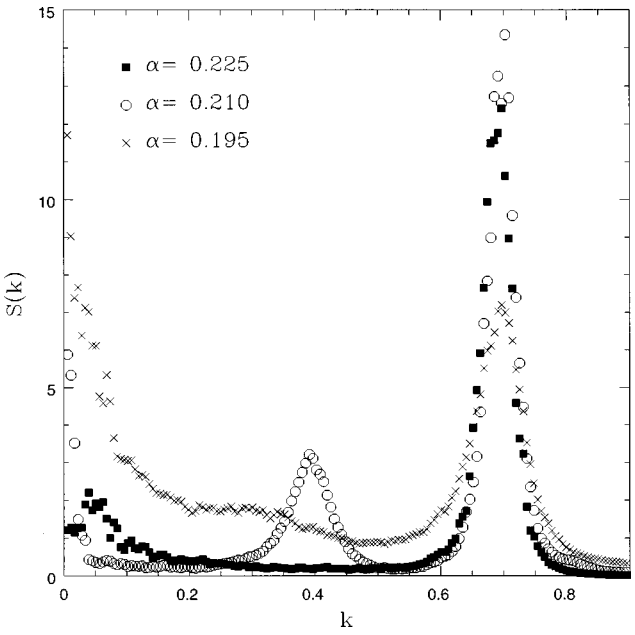

FIG. 3. Circularly averaged structure function $S(k)$ for the three states $\alpha=0.225$, 0.210, and 0.195.

averaged static structure factor $S(k)$ and the dynamic structure factor $S(k,w)$ were calculated,

$$S(k)=\sum_{|\vec{k}|=k}|\psi(\vec{k})|^2\Big/\sum_{|\vec{k}|=k}, \tag{4}$$

$$S(k,w)=\sum_{|\vec{k}|=k}|\psi(\vec{k},w)|^2\Big/\sum_{|\vec{k}|=k}. \tag{5}$$

The sum over $|\vec{k}|$ is a sum over all wave vectors with amplitude $|k|$ and $\hat{\psi}(\vec{k},w)$ is the discrete time Fourier transform of $\hat{\psi}(\vec{k},t)$,

$$\psi(\vec{k},w)=\sum_n e^{\sqrt{-1}wndt}\hat{\psi}(\vec{k},ndt). \tag{6}$$

The summation over iteration number n runs from $n=10^6$ to $n=10^6+327\,680$ in steps of $n=80$, i.e., $\hat{\psi}(\vec{k},ndt)$ was stored every 80 iterations starting from $n=10^6$ and ending at $n=10^6+327\,680$, and Fourier transformed to obtain $\psi(\vec{k},w)$. The static structure factor $S(k)$ was computed after 10^6 iterations and averaged over 10 different times, separated by 32 768 iterations.

$S(k)$ is shown for the three basic states in Fig. 3. The three different states are well characterized by $S(k)$. Three separate peaks centered around the wave vectors $k_D=0$, $k_B\approx0.39$, and $k_F\approx0.70$ can be distinguished. The peak at k_F is the fundamental peak corresponding to the basic periodicity of the hexagonal structure. The value of k_F is close to the wave vector that is most unstable in linear theory (i.e., $k_L=1/\sqrt{2}\approx0.707$). The width of the peak is inversely proportional to the average domain size, where a domain is defined as a region of ordered hexagons. Thus, in the large- and intermediate-α states, the peak is relatively sharp, while in the chaotic state it is quite broad. The peak centered at k_B is associated with the breathing mode and appears in the breathing and chaotic regimes. In addition to a peak at k_F, the breathing hexagonal pattern must have a peak at a longer wavelength to describe the larger unit cell that contains both a small and larger cell. Since this new cell size is roughly double the fundamental size, the peak appears at roughly half the value of k_F (the actual value of k_B is somewhat larger than this).

A clearer signature of the breathing mode is displayed by the dynamic structure factor. The dynamic structure factor was determined for a band of wave vectors centered around k_B; to improve statistics $S(k,w)$ was averaged over wave vectors in a small band centered around k_B (typically $\approx$ 100 wave vectors). The resultant average $S(k_Bw)$ is shown in Fig. 4 as a function of w for the three different states. This figure shows a well-defined peak at the frequency w_B, which decreases and broadens as α is reduced into the chaotic regime. The width of this peak is inversely proportional to the time over which the periodic oscillations are correlated. The state $\alpha=0.225$ in Fig. 4 corresponds to the hexagonal phase, where $S(k_B,w)$ is essentially zero compared to the breathing and chaotic state.

The k_D peak in the static structure factor $S(k)$ is associated with the defects in the patterns. To better highlight this feature it is convenient to diminish the short-wavelength fluctuations in ψ. A crude method to accomplish this is to coarse grain the configuration in real space by averaging over a block size or, equivalently, by filtering out the large-k fluctuations. To achieve this each pattern was Fourier transformed, multiplied by $S_D(k)/[S_D(k)+S_B(k)+S_F(k)]$, and inverse Fourier transformed. The functions $S_D(k)$, $S_B(k)$, and $S_F(k)$ were obtained by fitting the static structure factor $S(k)$ to the three peaks (k_D, k_B, and k_F, respectively). This technique effectively filters out the high-wave-vector behavior. The method works extremely well for the hexagonal states, but is only partially successful for the smaller α states. Some sample configurations are shown in

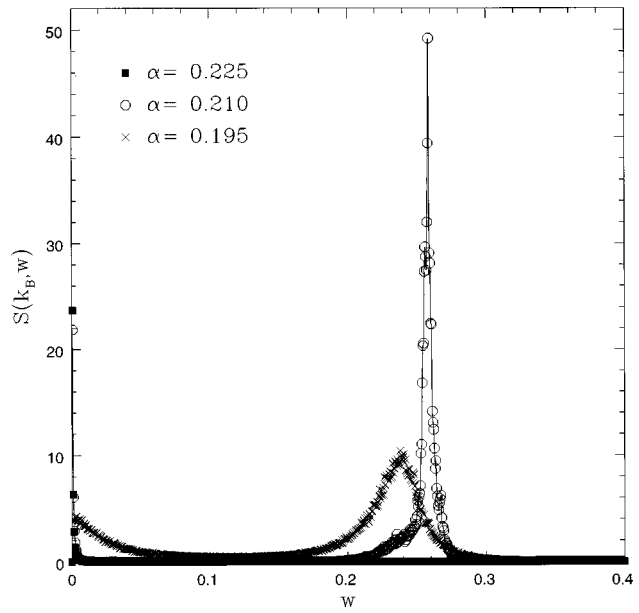

FIG. 4. Dynamic structure function $S(k_B,w)$ for the three states $\alpha=0.225$, 0.210, and 0.195. The length of the time series of the Fourier modes $\psi(\vec{k},t)$ is 4096 points, separated by 80 iterations, taken after $\approx 10^6$ iterations.

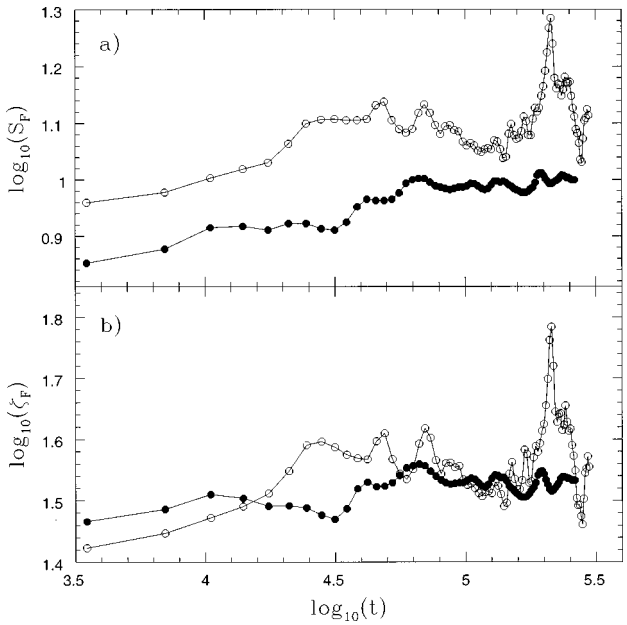

FIG. 5. Time dependence of the height of the (a) main peak S_F and (b) correlation length ζ_F. The open circles are for $\alpha=0.210$ and the closed circles for $\alpha=0.235$.

Figs. 1(d)–1(f). Comparing these with the raw configurations shown in Figs. 1(a)–1(c) illustrates the relationship between the defects and the small-k behavior of the structure function. Thus the small-wave vector behavior of $S(k)$ gives a description of the defect correlations.

By examining the real-space configurations as a function of α, it can be seen that the number of defects decreases as α approaches α_{CB}, from above and below. Comparing Figs. 1(d) and 1(e), it is evident that there are fewer defects for the breathing hexagonal state than for the larger-α hexagonal state. This is a somewhat surprising result, which presumably indicates that the true asymptotic states have not been reached for the hexagonal state. In fact, it is likely that the breathing states are closer to the true asymptotic states since the breathing modes act somewhat like fluctuations and allow the system to sample more states.

As with any numerical work it is difficult to determine whether the asymptotic regime has been reached. To examine this effect two runs were extended to $t=273\,000$ ($\approx 8\times 10^6$ iterations): one at $\alpha=0.210$ (i.e., a breathing state) and the other at $\alpha=0.235$ (i.e., a hexagonal state). Whereas the steady state for the spatiotemporal chaotic states seems to be reached within $t=35\,000$, the simulations for $\alpha=0.210$ and 0.235 indicate only a very small growth in the late stages ($t>35\,000$). In Fig. 5 the height of the fundamental peak $S_F\equiv S(k_F)$ and the correlation length ζ_F (defined to be the inverse of the width of the peak at half the maximum value) are shown for the two runs. This figure indicates that the system is ordering, but at a very slow (logarithmic at best) rate, with larger fluctuations for the smaller-α state. The number of defects does not seem to significantly decrease from one to 8×10^6 iterations; consequently, there is not much to be gained by extending the simulation times further. To assess whether the slow dynamics was influenced by the relatively large spatial grid and time steps used, test simulations were conducted at $dx=0.5$ and $dt=0.005$. No significant change in the system behavior was observed.

B. Transition points

In the one-dimensional damped Kuramoto-Sivashinsky equation there is strong evidence that the transition from periodic solutions to spatiotemporal chaos is discontinuous. In this subsection, the transition from hexagonal to breathing and from breathing to chaotic solutions is examined. As discussed in the preceding subsection, it is very difficult to examine the true asymptotic behavior due to the very slow dynamics. For this study the ''late'' stage (times $t\geqslant 35\,000$) solutions of the two-dimensional damped Kuramoto-Sivashinsky equation are studied as a function of α.

The states of the system were characterized by studying various properties of the peaks in the static and dynamic structure factors. The basic quantities that should characterize the hexagonal, breathing, and chaotic states are the inverse widths at half maximum (i.e., the correlation length ξ and correlation time τ) and the heights of the peaks in the static and dynamic structure factors. To facilitate the analysis, $S(k)$ was fit to three peaks with the form

$$S_D/(1+\zeta_D^2k^2)+S_B/[1+B(k^2-k_B^2)^2]$$

$$+S_F/[1+F(k^2-k_F^2)^2]$$

.

Similarly, the dynamic structure factor $S(k_B,w)$ was fit to $S_D^d/(1+\tau_0^2w^2)+S_B^d/[1+\gamma(w^2-w_0^2)^2]$. Sample fits are shown in Fig. 6 for $\alpha=0.206$. The quantities ζ_F, ζ_B, and τ_B were defined as the inverse of the widths of the peaks at $k=k_F$, $k=k_B$, and $w=w_B$, respectively.

The results of this study are presented in Figs. 7–9. The dashed vertical lines in these figures indicate the estimated transition points α_{CB} and α_{BO}. Data for the breathing mode (S_B, ζ_B, and k_B) are shown only for the interval

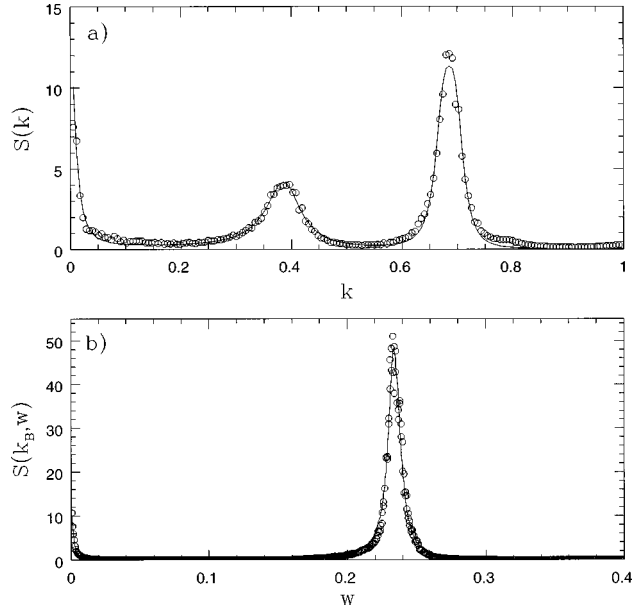

FIG. 6. Sample fit of the structure functions to Lorentzians for $\alpha=0.206$: (a) $S(k)$ fit and (b) $S(k_B,w)$ fit. Open circle symbols are the data points and the solid line is the fit.

$0.198<\alpha<0.217$, where a well-defined breathing mode peak can be distinguished. The parameters of the defect (small-k) peak are not displayed in these figures as the statistics are not reliable due to the poor resolution in the small-k regime.

In Fig. 7 the behaviors of S_F, S_B, and S_B^d are displayed. S_F is roughly constant above α_{CB} (although some small increase is seen near α_{CB}) and decreases below α_{CB}. Both S_B and S_B^d are approximately zero for $\alpha>\alpha_{BO}\approx 0.2176$, and peak sharply at $\alpha\approx\alpha_{CB}\approx 0.207$. The peak of the breathing mode excitation is a clear indicator of the transition to the chaotic state.

Figure 8 shows the correlation lengths of the static fundamental and breathing peaks ζ_F and ζ_B and the dynamic correlation time for the breathing peak τ_B, as a function of α. The correlation time τ_B decreases as α is decreased, but, aside from the larger scatter of data near α_{CB}, it does not exhibit a clear signature of the transition to spatiotemporal chaos. ζ_F and ζ_B both show a characteristic increase around α_{CB} to a more ordered state. It is also apparent that the correlation lengths are roughly constant near the breathing to hexagonal transition. A small peak in ζ_F seems to occur at the chaotic to breathing transition. The breathing hexagonal states for smaller α (i.e., close to α_{CB}) have a somewhat larger degree of translational order. This is consistent with the observation mentioned in Sec. III A that these states have fewer defects and are likely to be closer to their asymptotic state.

Figure 9 illustrates the behavior of k_F, k_B, and w as a function of α. Both k_B and w_B (in particular w_B) clearly mark the transition to spatiotemporal chaos. The typical pattern size $2\pi/k_F$ does not vary significantly as α is decreased

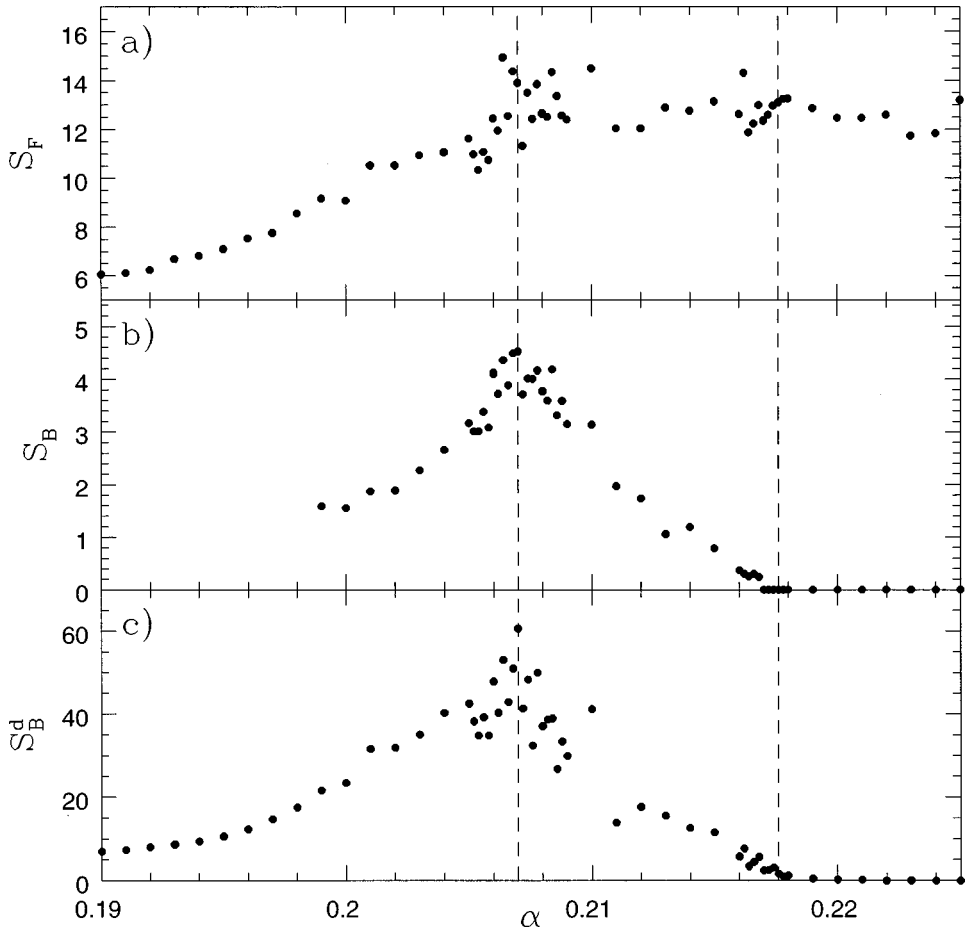

FIG. 7. (a) Height of the main peak S_F, (b) breathing mode peak S_B of the static structure factor as a function of α, and (c) height of the dynamic breathing mode peak S_B^d as a function of α.

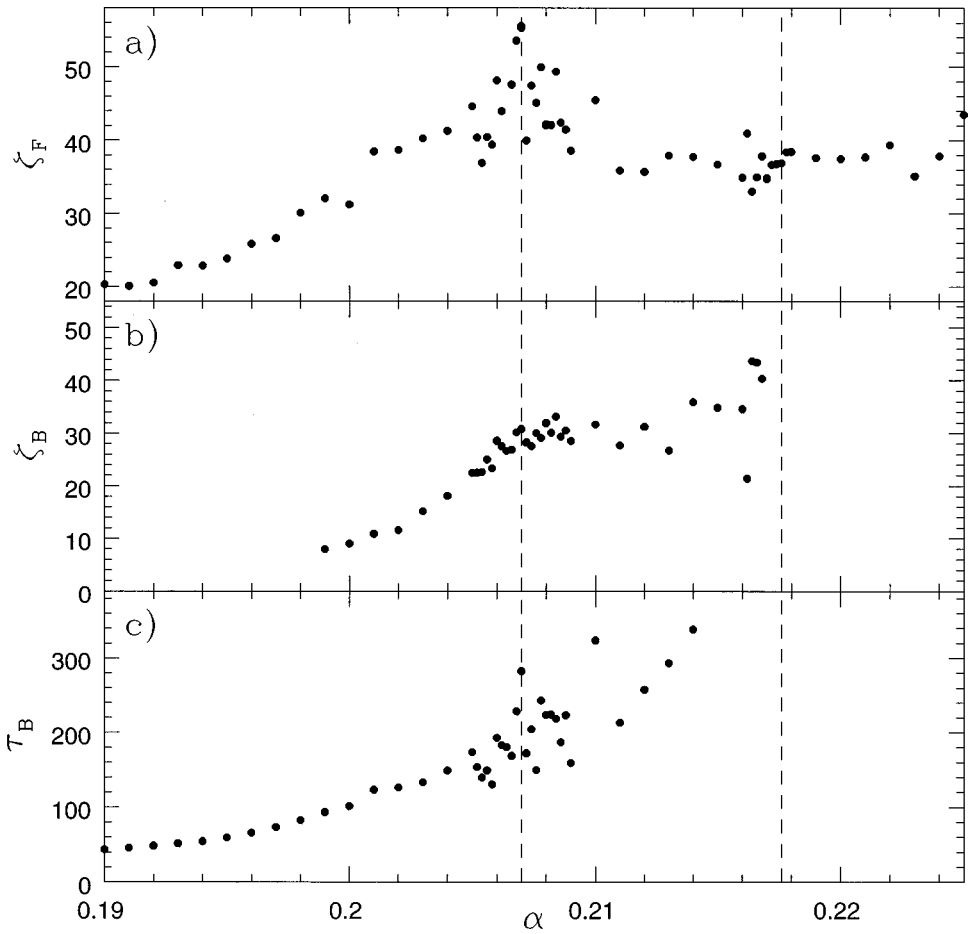

FIG. 8. Correlation lengths (a) ζ_F and (b) ζ_B and (c) the correlation time τ_B, as a function of α.

into the chaotic state. All the measured quantities in Figs. 7–9 appear to change continuously through the transition and give no indication of a discontinuity.

IV. DISCUSSION AND SUMMARY

In this paper the long-time behavior of the two-dimensional DKS equation was examined numerically in the large-aspect-ratio limit. The data presented indicated three distinct states: a hexagonal state for $\alpha > 0.2176$, a breathing hexagonal state for $0.207 < \alpha < 0.2176$, and a disordered or chaotic state for $\alpha < 0.207$. The states can be clearly distinguished using statistical quantities such as the widths and peak heights of the static and dynamic structure factor. Both the hexagonal and breathing hexagonal states are characterized by a sharp peak in the static structure factor at the fundamental wave vector. The breathing hexagonal state is distinguished from the hexagonal state by the appearance of a sharp peak in $S(k)$ at approximately half the fundamental wave vector and by a sharp peak in the dynamic structure factor. At small α spatiotemporal chaos occurs, which is characterized by diffuse peaks in both the static and dynamic structure factors. The transition between the chaotic state and breathing hexagonal state is highlighted by several quantities; most notably there is a significant peak in the amplitude of the breathing mode excitation (S_B and S_B^d) at $\alpha \approx \alpha_{CB}$.

While the results of these simulations cannot unambiguously determine the nature of the transition to spatiotemporal chaos, these results are somewhat reminiscent of a continuous phase transition. No discontinuities were observed in any measured quantities. This is in contrast to recent numerical simulations of the one-dimensional DKS equation in which a discontinuous transition to spatiotemporal chaos was observed. Nevertheless, it is important to note that it is computationally very expensive to establish the nature of this transition in two dimensions.

The main difficulty in determining the nature of the transition is in reaching the asymptotic states. While the present results indicate a smooth change from a breathing hexagonal state to spatiotemporal chaos, it is unknown whether this behavior will persist for the asymptotic (infinite time) states. Indeed, the basic question that arises is what the nature of the true asymptotic state is. It is easy to show numerically that perfect (defect-free) hexagonal states are stable (or at least metastable) solutions of the DKS equation at large α for a range of wave vectors. Unfortunately, there is no variational principle in this nonequilibrium dynamical system to determine if one of these states will be selected from random initial conditions.

In the absence of a general nonequilibrium selection scheme, it is interesting to consider what analogies with equilibrium behavior can be drawn. For an equilibrium system with a continuous symmetry, the lower critical dimension is $d=2$; for finite temperatures below T_c there is only quasi-long-range order [24]. The DKS has a continuous symmetry (translational and rotational symmetry), but the equa-

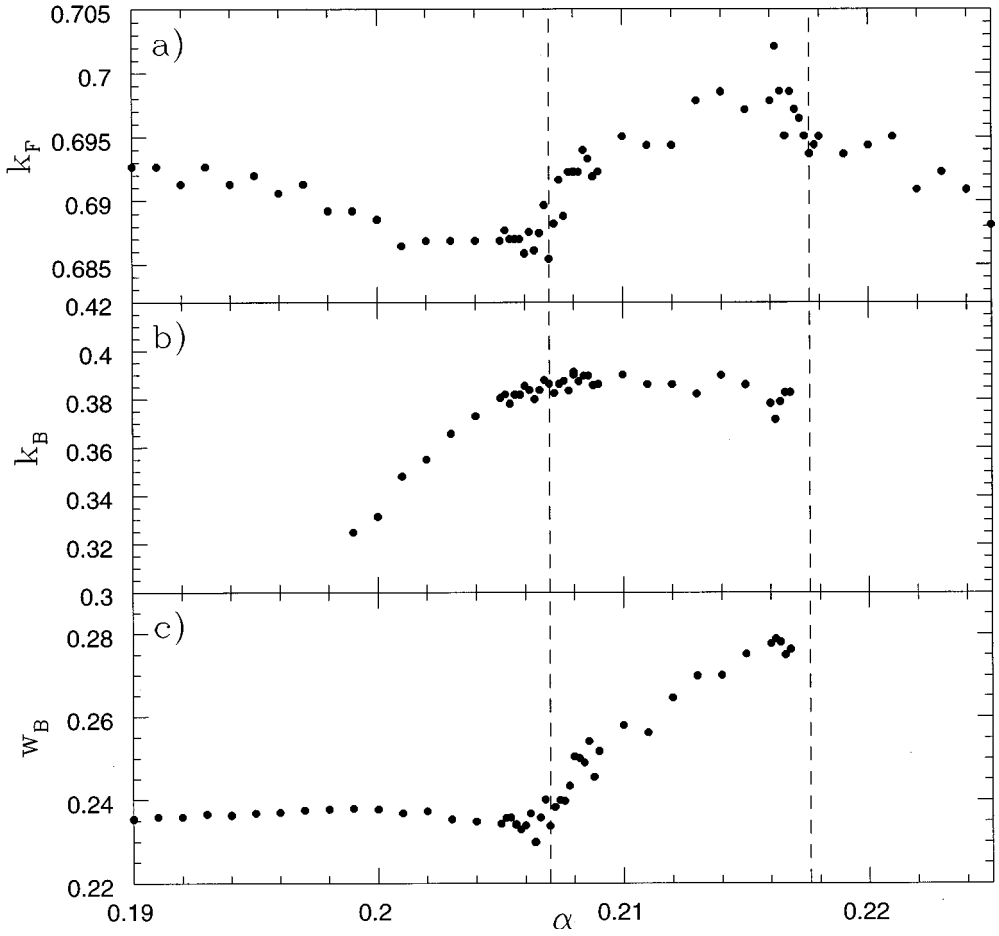

FIG. 9. Peak wave numbers (a) k_F and (b) k_B and (c) the peak frequency w_B, as a function of α.

tion is purely deterministic (zero noise). Thus the existence of a state with true long-range order is possible, as verified for $d=1$. Since it is easier to order a system for higher dimension (fluctuations are generally suppressed for higher d), it is likely that the two-dimensional DKS equation will evolve to a state with perfect long-range hexagonal order (for large α) at extremely long times. The existence of a state with long-range order in the DKS dynamics is then somewhat analogous to a zero-temperature equilibrium state.

To further this analogy, consider the secondary instabilities as a source of random noise. If this were the case, then the onset of the secondary instabilities would lead directly to spatiotemporal chaos in one dimension, as was observed in an earlier study [21]. As noted above, in two dimensions the appearance of thermal noise does not necessarily destroy the order (at least the system can have quasi-long-range order). Thus the persistence of the breathing hexagonal state for a finite range in α is presumably because the noise introduced via the breathing mode instability is not large enough to generate a chaotic state. Following the above reasoning, the equilibrium analogy for the DKS in $d=2$ should be closer to a Kosterlitz-Thouless-type [24] transition. This would mean that the asymptotic states for α in the breathing mode regime have no true long range order, but rather exhibit a power-law decay of correlation functions. This is an interesting conjecture that merits further study. We hope to perform larger-scale simulations in the future to investigate this model system further.

Finally, it is interesting to note that the same basic behavior was observed in parametrically driven surface waves. In this two-dimensional system, Zhang and Vinals [9] observed that the appearance of secondary instabilities (i.e., transverse amplitude modes) occurred before the onset of spatiotemporal chaos. Thus it is possible that the behavior observed in the two-dimensional DKS equation is more generic than might be expected for a nonequilibrium system.

ACKNOWLEDGMENTS

M.P. thanks Yoshi Oono for useful discussions and would like to acknowledge support by the National Science Foundation Grant No. NSF-DMR-93-14938. K.R.E. would like to acknowledge support from Research Corporation Grant No. CC4181.

[1] W. W. Mullins and R. F. Sererka, J. Appl. Phys. **35**, 444 (1964).
[2] J. S. Langer, Rev. Mod. Phys. **52**, 1 (1980).
[3] J. -M. Flesselles, A. J. Simon, and A. J. Libchaber, Adv. Phys. **40**, 1 (1991), and references therein.
[4] A. Valance, K. Kassner, and C. Misbah, Phys. Rev. Lett. **69**, 1544 (1992).
[5] B. Grossman, K. R. Elder, M. Grant, and J. M. Kosterlitz, Phys. Rev. Lett. **71**, 3323 (1993).
[6] Y. Hu, R. E. Ecke, and G. Ahlers, Phys. Rev. Lett. **74**, 391 (1995).
[7] S. W. Morris, E. Bodenshatz, D. S. Cannell, and G. Ahlers, Phys. Rev. Lett. **71**, 2026 (1993).
[8] H. W. Xi, J. D. Gunton, and J. Vinals, Phys. Rev. Lett. **71**, 2030 (1993).
[9] W. Zhang and J. Vinals, Phys. Rev. Lett. **74**, 690 (1995).
[10] A. Kudrolli and J. P. Gollub, Physica D **97**, 133 (1996).
[11] N. B. Tufillaro, R. Ramshankar, and J. P. Gollub, Phys. Rev. Lett. **62**, 422 (1989).
[12] M. Dennin, G. Ahlers, and D. S. Cannell, Phys. Rev. Lett. **77**, 2475 (1996); Science **272**, 388 (1996).
[13] J. Miles and D. Henderson, Annu. Rev. Fluid Mech. **22**, 143 (1990).
[14] M. C. Cross and P. C. Hohenberg, Rev. Mod. Phys. **65**, 851 (1993).
[15] P. C. Hohenberg and B. I. Shraiman, Physica D **37**, 109 (1989).
[16] M. Caponeri and S. Ciliberto, Physica D **58**, 365 (1992).
[17] C. Misbah and A. Valance, Phys. Rev. E **49**, 166 (1994).
[18] H. Chaté and P. Manneville, Phys. Rev. Lett. **58**, 112 (1987).
[19] A. Novick-Cohen and G. I. Sivashinsky, Physica D **20**, 237 (1986).
[20] I. Bena, C. Misbah, and A. Valance, Phys. Rev. E **47**, 7408 (1993).
[21] K. R. Elder, J. D. Gunton, and N. Goldenfeld, Phys. Rev. E. **56**, 1631 (1997).
[22] P. Manneville, *Dissipative Structures and Weak Turbulence* (Academic, New York, 1990).
[23] Y. Oono and S. Puri, Phys. Rev. Lett. **58**, 836 (1987).
[24] J. M. Kosterlitz and D. J. Thouless, J. Phys. C **6**, 1181 (1973).